NJC

PAPER

View Article Online
View Journal

Cite this: DOI: 10.1039/c5nj01899d

Supramolecular frameworks of binuclear dioxomolybdenum(VI) complexes with ONS donor ligands using 4,4′-azopyridine as a pillar: crystal structure, DFT calculations and biological study†

Debanjana Biswal,[a] Nikhil Ranjan Pramanik,*[b] Syamal Chakrabarti,*[a] Michael G. B. Drew,[c] Payel Mitra,[d] Krishnendu Acharya,[d] Sujan Biswas[e] and Tapan Kumar Mondal[e]

Received (in Victoria, Australia) 20th July 2015,
Accepted 26th August 2015

DOI: 10.1039/c5nj01899d

www.rsc.org/njc

Three new isostructural pillared binuclear dioxomolybdenum(VI) complexes $[(MoO_2L^1)_2(4,4'\text{-azpy})]$ (**1**), $[(MoO_2L^2)_2(4,4'\text{-azpy})]$ (**2**) and $[(MoO_2L^3)_2(4,4'\text{-azpy})]$ (**3**) [where, 4,4′-azpy = 4,4′-azobis-(pyridine)] containing tridentate binegative Schiff base ligands (H_2L^1, H_2L^2 and H_2L^3) obtained by the condensation of salicylaldehyde and substituted salicylaldehyde with *S*-benzyl dithiocarbazate have been reported for the first time. These complexes have been characterized by spectroscopic and electrochemical studies. In all the complexes (**1–3**), 4,4′-azpy behaves as an auxiliary spacer and bridges the Mo(VI) centers giving rise to neutral 3D supramolecular frameworks. The cavities formed by hydrogen bonding interactions are capable of hosting guest molecules. The crystal structures reveal that each molybdenum site in the binuclear complexes adopts a distorted octahedral geometry. The morphology and structures of the complexes are further examined by SEM. Thermal behavior has been investigated to study the framework stabilities of these structures. Supportive DFT calculations on the complexes have been carried out. These ligands and complexes **1–3** have significant antimicrobial and antioxidant properties.

Introduction

Molybdenum chemistry has become a prospective area of research because of the presence of molybdenum in metalloenzymes and its significant role in hydroxylase and oxo-transferase enzymes[1–7] and due to the possible antifungal,[8] antibacterial,[9] antitumor[10] and antiviral[11] properties of molybdenum complexes. Molybdenum complexes are used as effective catalysts in industry[12–14] and oxidation reactions[15] because they possess a large number of stable and accessible oxidation states as well as coordination numbers. Numerous mononuclear dioxomolybdenum(VI) complexes have been reported but the crystal structures of few binuclear Mo(VI) complexes with ONS donor ligands have been determined so far.[16–19] The construction of coordination complexes with new network motifs is of current interest for the development of functional materials and in fundamental studies of crystal engineering and supramolecular chemistry.[16,20–22] Supramolecular frameworks involving organic bridging ligands[23] acting as spacers have been an interesting area of research. Hydrogen bonding plays a significant role in supramolecular assemblies with structural diversity and potential applications in various fields such as selective gas-adsorption,[24] separation,[25] drug delivery[26] and catalysis[27] because of its dimensional nature and strength.

Pyridine and its derivatives have been very useful monodentate ligands in many aspects of coordination chemistry.[28] Bipyridyl bridging ligands incorporating alkane, alkene and alkyne functionalities have been widely used for the construction of binuclear complexes.[16,29,30] Neutral N-donor ligands are often used as auxiliary ligands owing to their affinities to transition metal ions and conformations as pillar-like connectors.[31] These auxiliary ligands play an important role in controlling the topology and

[a] Department of Chemistry, University College of Science, 92, Acharya Prafulla Chandra Road, Kolkata-700009, West Bengal, India. E-mail: schakrabarti2014@gmail.com; Fax: +91 033-2351-9755; Tel: +91 033-2350-8386
[b] Department of Chemistry, Bidhannagar College, EB-2,Sector-1, Salt Lake, Kolkata-700064, India. E-mail: nr_pramanik@yahoo.co.in; Fax: +91 033-2337-4782; Tel: +91 033-2337-4389
[c] Department of Chemistry, The University of Reading, Whiteknights, Reading RG66AD, UK
[d] Molecular and Applied Mycology and Plant Pathology Laboratory, Department of Botany, University of Calcutta, Kolkata 700019, West Bengal, India
[e] Department of Chemistry (Inorganic section), Jadavpur University, Kolkata 700032, India

† Electronic supplementary information (ESI) available: Fig. S1–S8 contain cyclic voltammograms, TG–DT curves, various supramolecular architectures, and Tables S1–S3 contain the energy and composition of selected molecular orbitals of complexes **1–3**. CCDC 1054805, 1054806 and 1054804. For ESI and crystallographic data in CIF or other electronic format see DOI: 10.1039/c5nj01899d

dimensionality of the resultant supramolecular frameworks containing cavities or channels which are crucial for thermal stability. However, the coordination properties of closely related bipyridyl ligands comprising the azo (–N=N–) functional moiety, namely 4,4′-azopyridine have received less attention. Therefore, the construction of complexes containing 4,4′-azpy as an auxiliary ligand should be very interesting from the structural viewpoint.

A search of the Cambridge Crystallographic Database shows that complexes involving the 4,4′-azpy spacer have been reported previously with many transition metals,[32] but not so far including molybdenum. It is to be noted that no literature examples of the use of 4,4′-azpy as a pillaring spacer with $[MoO_2L]$ (L = ONS donor Schiff base ligand) in supramolecular framework syntheses exist. Herein, we report for the first time the 4,4′-azpy spacer for the fabrication of three new isostructural dioxomolybdenum(VI) binuclear pillar complexes **1–3** with ONS donor ligands. In these complexes non-covalent interactions play a pivotal role in the construction of fascinating neutral 3D supramolecular networks. The 4,4′-azpy spacer is particularly useful in that because it can provide enough space to create cavities. The presence of interaction sites on the pore surface enhances guest anchoring. The solid state molecular structures of complexes **1–3** have been ascertained by single-crystal X-ray diffraction methods. Each Mo site in the binuclear complexes adopts an octahedral geometry. The structures contain two $[MoO_2]^{2+}$ moieties bridged by two nitrogen atoms from the 4,4′-azpy spacer. The details of the crystal structures, host–guest interactions, and framework stability are discussed later. The morphology of the complexes is examined by SEM. Their thermal and electrochemical behaviors have been investigated. Supportive DFT calculations on the complexes have been carried out in order to obtain deeper insight into the electronic situation around the molybdenum centre. The significant antimicrobial and antioxidant activities of these ligands and investigated complexes have also been examined.

Experimental section

Materials

Reagent grade solvents were dried and distilled prior to use. 4,4′-Azobis-(pyridine) (4,4′-azpy) was prepared as an orange solid by the procedures reported previously.[33] All other chemicals used for the preparative work were of reagent grade, available commercially and used without further purification.

Synthesis

Synthesis of the ligands

The Schiff base ligands $\mathbf{H_2L^1}$, $\mathbf{H_2L^2}$ and $\mathbf{H_2L^3}$ were prepared by condensing *S*-benzyl dithiocarbazate with salicylaldehyde, 5-nitro-salicylaldehyde and 5-bromosalicylaldehyde in ethanol by methods reported previously[34] (Scheme 1). The ligands were satisfactorily characterized by elemental analyses, IR and ^{1}H NMR.

***S*-Benzyl-β-*N*-(2-hydroxyphenyl)methylenedithiocarbazate ($\mathbf{H_2L^1}$).** Anal. calc. for $C_{15}H_{14}S_2N_2O$ (%): C, 59.60; H, 4.64; N, 9.30, found: C, 59.71; H, 4.80; N, 9.43, IR (KBr Pellet), cm^{-1}: $\nu_{(O-H)}$ 3425(m), $\nu_{(N-H)}$ 3100(m), $\nu_{(C=N)}$ 1617(s), 1604(s), $\nu_{(C=S)}$ 1311(s); ^{1}H NMR($CDCl_3$): (–S–CH_2–) 4.59 s (2H), (aromatic protons) 6.92–7.43 m (9H), (H–C=N) 8.04 s (1H), (–NH–) 10.02 s (1H), (aromatic –OH) 10.72 s (1H).

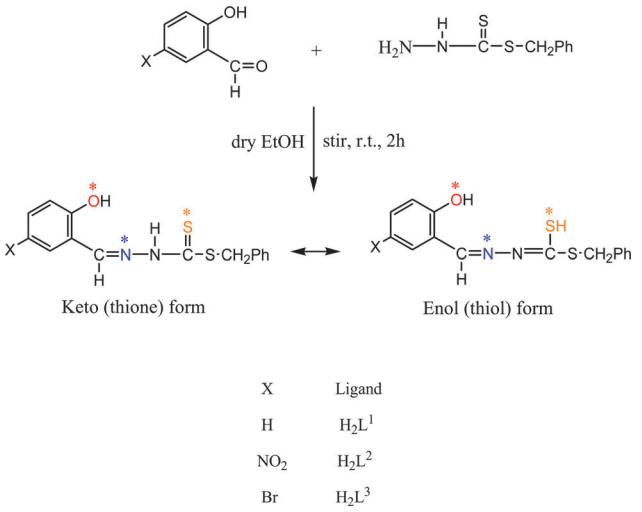

X	Ligand
H	H_2L^1
NO_2	H_2L^2
Br	H_2L^3

Scheme 1 Reaction diagram for isolation of the ligands.

***S*-Benzyl-β-*N*-(5-nitro-2-hydroxyphenyl)methylenedithiocarbazate ($\mathbf{H_2L^2}$).** Anal. calc. for $C_{15}H_{13}S_2N_3O_3$ (%): C, 51.87; H, 3.74; N, 12.10, found: C, 51.65; H, 3.70; N, 12.00, IR (KBr Pellet), cm^{-1}: $\nu_{(O-H)}$ 3081(m), $\nu_{(N-H)}$ 2952(m), $\nu_{(C=N)}$ 1626(s), 1602(s), $\nu_{(C=S)}$ 1339(vs); ^{1}H NMR ($CDCl_3$): (–S–CH_2–) 4.62 s (2H), (aromatic protons) 7.08–7.43 m (8H), (H–C=N) 8.06 s (1H), (–NH–) 10.41 s (1H), (aromatic –OH) 10.81 s (1H).

***S*-Benzyl-β-*N*-(5-bromo-2-hydroxyphenyl)methylenedithiocarbazate ($\mathbf{H_2L^3}$).** Anal. calc. for $C_{15}H_{13}S_2N_2OBr$ (%): C, 47.24; H, 3.41; N, 7.34, found: C, 47.10; H, 3.35; N, 7.28, IR (KBr Pellet), cm^{-1}: $\nu_{(O-H)}$ 3102(m), $\nu_{(N-H)}$ 2973(m), $\nu_{(C=N)}$ 1615(s), 1603(s), $\nu_{(C=S)}$ 1324(vs); ^{1}H NMR ($CDCl_3$): (–S–CH_2–) 4.60 s (2H), (aromatic protons) 6.88–7.49 m (8H), (H–C=N) 7.91 s (1H), (–NH–) 10.25 s (1H), (aromatic –OH) 11.28 s (1H).

Synthesis of the complexes

All the mononuclear MoO_2L complexes were prepared by refluxing $MoO_2(acac)_2$ and the respective ligands in dry chloroform for 2 h. The complexes were satisfactorily characterized by elemental analyses, IR and ^{1}H NMR.[34]

$[(MoO_2L^1)_2(4,4'\text{-azpy})]\cdot 2CHCl_3$ (1). A mixture of 0.856 g (2 mmol) of MoO_2L and 0.184 g (1 mmol) of 4,4′-azobis-(pyridine) in dry $CHCl_3$ (20 mL) was refluxed for 3 h. The solution was filtered. Shiny orange-red single crystals suitable for X-ray diffraction analysis were obtained after one day. Yield ~70%. Anal. calc. for $C_{42}H_{34}S_4N_8O_6Cl_6Mo_2$ (%): C, 39.41; H, 2.65; N, 8.75; Mo, 15.01, found: C, 39.35; H, 2.54; N, 8.69; Mo, 14.92, IR (KBr Pellet), cm^{-1}: $\nu_{(C=N)}$ 1599(vs), $\nu_{(Mo=O)}$ 930(vs), 900(s), $\nu_{(Mo-N)}$ 635(s), $\nu_{(Mo-S)}$ 430(m); UV-Vis (CH_2Cl_2) [λ_{max}/nm (ε/dm^3 mol^{-1} cm^{-1})]: 299 (5740), 403 (1710); ^{1}H NMR ($CDCl_3$): (–S–CH_2–Ph) 4.43 s (4H), (aromatic protons) 7.22–7.68 m (26H), (H–C=N) 9.09 s (2H).

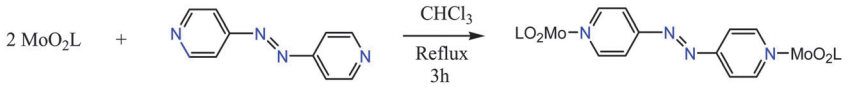

Scheme 2 Reaction diagram for the synthesis of $(MoO_2L)_2$(4,4′-azpy) complexes.

Complexes **2** and **3** were prepared similarly by refluxing the corresponding parent MoO_2L complex with 4,4′-azopyridine (4,4′-azpy) in a 2 : 1 molar ratio in dry $CHCl_3$ for 3 h. (Scheme 2). The solution was filtered. Shiny orange-red single crystals suitable for X-ray diffraction analysis were obtained after one day. Yield ~70–75%.

$[(MoO_2L^2)_2(4,4'\text{-azpy})]\cdot 2CHCl_3$ (2). Anal. calc. for $C_{42}H_{32}S_4N_{10}O_{10}Cl_6Mo_2$ (%): C, 36.81; H, 2.33; N, 10.22; Mo, 14.02, found: C, 36.75; H, 2.30; N, 10.18; Mo, 14.00, IR (KBr Pellet), cm^{-1}: $\nu_{(C=N)}$ 1597(vs), $\nu_{(Mo=O)}$ 935(vs), 902(s), $\nu_{(Mo-N)}$ 664(s), $\nu_{(Mo-S)}$ 446(m); UV-Vis (CH_2Cl_2) [λ_{max}/nm (ε/dm^3 mol^{-1} cm^{-1})]: 294 (8730), 404 (1270); ^{1}H NMR ($CDCl_3$): (–S–CH_2–Ph) 4.47 s (4H), (aromatic protons) 7.28–7.73 m (24H), (H–C=N) 8.85 s (2H).

$[(MoO_2L^3)_2(4,4'\text{-azpy})]\cdot 2CHCl_3$ (3). Anal. calc. for $C_{42}H_{32}S_4N_8O_6Cl_6Br_2Mo_2$ (%): C, 35.07; H, 2.22; N, 7.79; Mo, 13.36, found: C, 34.89; H, 2.17; N, 7.72; Mo, 13.01, IR (KBr Pellet), cm^{-1}: $\nu_{(C=N)}$ 1593(vs), $\nu_{(Mo=O)}$ 932(vs), 901(s), $\nu_{(Mo-N)}$ 659(s), $\nu_{(Mo-S)}$ 435(m); UV-Vis (CH_2Cl_2) [λ_{max}/nm (ε/dm^3 mol^{-1} cm^{-1})]: 298 (9110), 353 (4210); ^{1}H NMR ($CDCl_3$): (–S–CH_2–Ph) 4.42 s (4H), (aromatic protons) 7.28–7.75 m (24H), (H–C=N) 8.84 s (2H).

Physical measurements

Elemental analyses were performed on a Perkin-Elmer 240 C, H, N analyzer. NMR spectra were recorded on a Bruker 300 L NMR spectrometer operating at 300 MHz using TMS as internal standard. IR spectra were recorded as KBr pellets on a Perkin-Elmer model 883 infrared spectrophotometer. Electronic spectra were recorded using a HITACHI U-3501 UV-Vis recording spectrophotometer. Magnetic susceptibility was measured on a PAR model 155 vibrating sample magnetometer using $Hg[Co(SCN)_4]$ as a calibrant. Electrochemical data were collected on a Sycopel model AEW2 1820 F/S instrument at 298 K using a Pt working electrode, a Pt auxiliary electrode and a SCE reference electrode. Cyclic voltammograms were recorded in DMF containing 0.1 M TBAP as a supporting electrolyte. Thermal analyses were carried out on a NETZSCH STA 449 F3 Jupiter thermal analyzer in a dynamic atmosphere of dinitrogen (flow rate = 30 cm^3 min^{-1}). SEM images of the complexes were collected using an EVO 50 scanning electron microscope from ZEISS. The operating voltage and magnification were kept at 20 kV and 10 000×, respectively throughout the study.

Crystallographic measurements

The crystallographic data for complexes **1** and **3** were collected on a Bruker APEX-II diffractometer equipped with a CCD-area detector, and for complex **2** was collected on an Oxford Diffraction X-Calibur System. All data sets were obtained with graphite-monochromated Mo-Kα (λ = 0.71073 Å) radiation. Unit-cell dimensions and intensity data for **1**, **2** and **3** were measured at 296(2), 150(2) and 296(2) K, respectively. Data analysis for **1** and **3** were carried out using SAINT[35] and for **2** using the CrysAlis program.[36] The crystal structures were solved by direct methods using SHELXS-97[37] and refined by full-matrix least-squares based on F^2 with anisotropic displacement parameters of non-hydrogen atoms using SHELXL-97.[37] The hydrogen atoms were included in calculated positions. All three structures contained solvent chloroform disordered over two superimposed sites. These molecules were necessarily refined with distance constraints. Thermal parameters in the bridging ligand in **3** were high but no pattern of disorder could be identified. Absorption corrections for **1** and **3** were carried out using SADABS[38] and for **2** using ABSPACK.[39] The MERCURY[40] and DIAMOND[41] programs were used for the presentation of the structures.

Computational details

Full geometry optimization of **1**, **2** and **3** were carried out using the DFT method at the B3LYP level of theory.[42,43] The LanL2DZ basis set with an effective core potential was employed for the molybdenum atom.[44–46] The 6-31+G(d) basis set was assigned for all other elements. The vibrational frequency calculations were performed to ensure that the optimized geometries represent the local minima on the potential energy surface with only positive eigen-values. The lowest 50 singlet–singlet vertical electronic excitations based on B3LYP optimized geometries were computed using the time-dependent density functional theory (TDDFT) formalism[47–49] in CH_2Cl_2 using a conductor-like polarizable continuum model (CPCM)[50–52] using the same methodology. All computations were performed using the Gaussian09 (G03) program.[53] GaussSum[54] was used to calculate the fractional contributions of various groups to each molecular orbital.

Antimicrobial activity

Test organisms. All the test human pathogenic microorganisms *Escherichia coli* MTCC CODE 68, *Bacillus subtilis* MTCC CODE 736, *Listeria monocytogenes* MTCC 657, *Staphylococcus aureus* MTCC 96 were obtained from the culture collection of the Microbial Type Culture Collection and Gene Bank (MTCC), Institute of Microbial Technology, Chandigarh, India.

Screening of antimicrobial activity by the disk diffusion method. Antimicrobial activities of the ligands and complexes **1–3** were determined by the agar-disk diffusion method.[55] *Listeria monocytogenes* MTCC 657 and *Bacillus subtilis* MTCC 121 were incubated at 28 °C for 1 day by inoculation in nutrient broth. *Escherichia coli* MTCC 1667 and *Staphylococcus aureus* MTCC 96 were incubated at 37 °C. Nutrient agar was poured into each sterilized Petri dish (90 mm diameter) after injecting cultures (100 μl) of bacteria (10^6 cfu ml^{-1}) medium were distributed homogeneously. For the investigation of the antibacterial activity, filter paper disks (6 mm in diameter) were impregnated with individual compounds dissolved in 50% DMSO in order to

reach the final levels of 10 μg per disk. The impregnated discs were air dried before placing them on the Petri dishes with the test microorganisms and the plates were incubated at 37 °C. Discs with only 50% DMSO were used as negative controls. Standard antibiotic discs with tetracycline (10 μg per disc) and ampicillin (10 μg per disc) were used as positive controls. The mean values obtained for three individual replicates were used to calculate the zone of growth inhibition which was measured in mm using clear a graduated ruler. Studies were performed in triplicate.

Determination of minimal inhibitory concentration (MIC). The MIC study was aimed to find out the lowest concentration of the sample that inhibits the growth of the test organisms. The test was carried out using the filter paper disc method with varying concentrations of the synthesized compounds placed on bacteria. The plates were incubated for 24 h at 37 ± 0.1 °C and 28 ± 0.1 °C as required for the pathogens and the MIC recorded as the lowest concentration at which no growth was observed.

Antioxidant activity

Total antioxidant capacity assay. The assay is based on the reduction of Mo(VI) to Mo(V) by the extract; as was done by Prieto *et al.*[56] When an acidic pH is maintained subsequent formation of a green phosphate/Mo(V) complex is seen. The tubes containing compounds (ligands and complexes **1–3**) and reagent solution (0.6 M sulfuric acid, 28 mM sodium phosphate and 4 mM ammonium molybdate) were incubated at 95 °C for 90 min. Then, the mixture was cooled to room temperature. The absorbance was recorded spectrophotometrically for each solution at 695 nm against a blank.

DPPH radical-scavenging activity. As per the method of Shimada *et al.*[57] 0.004% methanolic solution of DPPH (2,2-diphenyl-1-picrylhydrazyl) was prepared. Then, various concentrations of the compounds (ligands and complexes **1–3**) were added to it. The mixture was shaken vigorously and left to stand for 30 min in the dark. Gradual fading of a purple colour were measured at 517 nm against a blank. Ascorbic acid was used as a positive control. The degree of scavenging was calculated using the following equation:

$$\text{Scavenging effect (\%)} = \{(A_0 - A_1)/A_0\} \times 100$$

Where A_0 is the absorbance of the control and A_1 is the absorbance if the sample is present.

Results and discussion

Synthesis

The Schiff base ligands $\mathbf{H_2L^1}$, $\mathbf{H_2L^2}$ and $\mathbf{H_2L^3}$ were prepared by condensing *S*-benzyl dithiocarbazate with salicylaldehyde, 5-nitrosalicylaldehyde and 5-bromosalicylaldehyde in ethanol. The ligands were satisfactorily characterized by elemental analyses, IR and ^{1}H NMR.

All the binuclear Mo(VI) complexes (**1–3**) with general formula $[(MoO_2L)_2(4,4'\text{-azpy})]$ were prepared by refluxing the corresponding parent MoO_2L complex with 4,4′-azpy in a 2 : 1 molar ratio in dry chloroform.

All the orange-red binuclear dioxomolybdenum(VI) complexes (**1–3**) are air stable in the solid state. The compounds are readily soluble in alcohol, CH_2Cl_2, CH_3CN, DMF and DMSO but are insoluble in water. The complexes are diamagnetic at room temperature as expected for d^0Mo(VI) centers.[58] Molar conductivity data in 10^{-3} M CH_2Cl_2 solution indicate that they are non-electrolytes. All the binuclear Mo(VI) complexes are satisfactorily characterized by elemental analyses, IR, ^{1}H NMR, electronic spectra and cyclic voltammetry. The complexes **1–3** have been structurally characterized by single crystal X-ray diffraction.

IR and ^{1}H NMR spectra

Characteristic IR bands of the ligands and the corresponding binuclear molybdenum(VI) complexes (**1–3**) are given in the Experimental section. The ligands ($\mathbf{H_2L^1}$, $\mathbf{H_2L^2}$ and $\mathbf{H_2L^3}$) exhibit two broad bands of medium intensity in the 3425–3081 cm^{-1} range due to the $\nu_{(O-H)}$ mode and the 3100–2952 cm^{-1} range is assigned to the $\nu_{(N-H)}$ vibration.[59] Strong $\nu_{(C=N)}$ bands[60,61] at around 1620 cm^{-1} of the free ligands are red shifted to 1599 cm^{-1}, 1597 cm^{-1} and 1593 cm^{-1}, respectively, in the corresponding complexes indicating the coordination of azomethine nitrogen to the metal ion. Strong $\nu_{(C=S)}$ bands observed in 1311–1339 cm^{-1} region for the ligands, which disappeared on complex formation indicating the coordination of thioenolate sulfur to the $[MoO_2]^{2+}$ centre. Bands at 635–664 cm^{-1} for the complexes are assigned to $\nu_{(Mo-N)}$.[62] Medium intensity bands for the complexes at around 430–446 cm^{-1} are assigned to $\nu_{(Mo-S)}$.[63] The complexes exhibit two very strong $\nu_{(Mo=O)}$ bands in the region 900–935 cm^{-1}, characteristic of the symmetric and antisymmetric stretching vibrations of the *cis*-$[MoO_2]^{2+}$ moiety.[64,65]

^{1}H NMR data for the ligands and the corresponding complexes (**1–3**) in $CDCl_3$ are summarized in the Experimental section. The relatively broad signals at δ 10.72 and δ 10.02 ppm; δ 10.81 and δ 10.41 ppm; δ 11.28 and δ 10.25 ppm in the ^{1}H NMR spectra corresponding to the O–H and N–H bonds of ligands $\mathbf{H_2L^1}$, $\mathbf{H_2L^2}$ and $\mathbf{H_2L^3}$ are found to disappear in the complexes **1**, **2** and **3**, respectively, as a result of complexation. The signals at δ 8.04, δ 8.06 and δ 7.91 ppm of the ligands shift downfield to δ 9.09, δ 8.85 and δ 8.84 ppm indicating coordination from the azomethine nitrogen in the complexes. The methylene protons of the ligands and their corresponding complexes **1**, **2** and **3** appearing at δ 4.59 and δ 4.43 ppm; δ 4.62 and δ 4.47 ppm; δ 4.60 and δ 4.42 ppm indicate that the *S*-benzyl sulfur is not involved in the coordination. In ligand $\mathbf{H_2L^1}$, nine aromatic protons, and in ligands $\mathbf{H_2L^2}$ and $\mathbf{H_2L^3}$ eight aromatic protons appear as multiplets within the ranges δ 6.92–7.43 ppm, δ 7.08–7.43 ppm and δ 6.88–7.49 ppm, respectively. In complex **1**, 26 and in complexes **2** and **3**, 24 aromatic protons appear as multiplets within the ranges δ 7.22–7.68 ppm, δ 7.28–7.73 ppm and δ 7.28–7.75 ppm, respectively.

Considering the IR and ^{1}HNMR data together, it is observed that both the data support each other in respect to the donor sites of the ligands through which they coordinate to the $[MoO_2]^{2+}$ centre.

Electronic spectra

Electronic spectra of the binuclear dioxomolybdenum(VI) (**1–3**) complexes were recorded in dry CH_2Cl_2 and the spectral data are listed in the Experimental section. Spectra of all the binuclear $[(MoO_2L)_2(4,4'\text{-azpy})]$ complexes exhibit several bands in the 404–294 nm range. All the complexes display the lowest energy absorption maxima in the 404–353 nm range which are assigned[66] to a S(pπ) → Mo(dπ) LMCT transition involving the promotion of an electron from the filled HOMO of the ligand to the empty LUMO of Mo. Other LMCT bands which may be assigned to nitrogen to molybdenum and oxygen to molybdenum charge transfer transitions are observed in the 299–294 nm range.[66–69]

Electrochemical properties

Cyclic voltammograms of the binuclear $[(MoO_2L)_2(4,4'\text{-azpy})]$ complexes (**1–3**) at a platinum electrode were recorded in dry degassed DMF containing 0.1 M TBAP as the supporting electrolyte over the potential range 0.0 to −1.5 V. The cyclic voltammetric results of all the binuclear dioxomolybdenum(VI) complexes are given in Table 1 and the cyclic voltammograms are shown in Fig. S1 (ESI†). All the complexes show only one irreversible two-electron one-step reduction within the potential range −0.92 to −1.01 V *vs.* the SCE in DMF solution which corresponds to a Mo^{VI}–Mo^{VI}/Mo^{IV}–Mo^{IV} couple.[15,70] Two-electron involvement is established by a comparison of the current height with authentic two electron species under identical experimental conditions. On scan reversal, one irreversible two-electron one step oxidative response is located in the range 0.44 to 0.47 V which corresponds to a Mo^{IV}–Mo^{IV}/Mo^{VI}–Mo^{VI} couple. It should be noted that the reduction of binuclear $[(MoO_2L)_2(4,4'\text{-azpy})]$ complexes in aprotic solvents is generally irreversible.

Thermogravimetric analysis and framework stability

Thermogravimetric analyses of complexes **1–3** were conducted in the temperature range 30–700 °C with a 10 °C min^{-1} interval in nitrogen atmosphere to assess their framework stabilities (Fig. S2–S4, ESI†). Above 200 °C, the TG/DTA curve exhibits three steps of weight loss. Complex **1** shows a weight loss of ∼8% supported by an exothermic peak around 210–220 °C, which corresponds to the loss of one guest solvent $CHCl_3$ molecule (calc. 9.3%) and the framework is quite stable up to 275 °C. In the temperature range 275–330 °C, a ∼30.19% weight loss was observed suggesting the concomitant loss of the second solvent $CHCl_3$ molecule and the 4,4′-azpy spacer (calc. 33.05%). In the third step above 600 °C, a ∼47.31% weight loss was observed suggesting the removal of two molecules of $-CH_2Ph$ ligand fragments (calc. 47.28%). Upon further heating the compound decomposes to an unidentified product.

Complexes **2** and **3** show a weight loss of ∼8% supported by an exothermic peak around 210–220 °C which corresponds to the loss of one guest $CHCl_3$ molecule [calc. 8.7% (**2**) and 8.31% (**3**)]. The second weight losses of ∼16% (**2**) and ∼18.1% (**3**) start around 275–330 °C suggesting the loss of the second guest $CHCl_3$ molecule [calc. 17.45% (**2**) and 16.62% (**3**)]. Finally, the major weight loss of ∼38.1% (**2**) and ∼45.9% (**3**) occurring until ∼600 °C corresponds to the loss of the 4,4′-azpy spacer along with two molecules of $-CH_2Ph$ ligand fragments [calc. 40.17% (**2**) and 42.09% (**3**)]. This suggests retention of the framework structures of **2** and **3** up to ∼600 °C indicating the robustness of the framework even after the removal of the guest $CHCl_3$ molecules.

Thus, the thermogravimetric study reveals that with minor variations between the curves, all the complexes show similar decomposition profiles because of the similarities in the metal coordination modes in the structures.

Description of the crystal structures of complexes 1, 2 and 3

The molecular structures and the atom numbering schemes of complexes **1**, **2** and **3** are shown in Fig. 1–3. Crystallographic data, relevant bond lengths and bond angles together with hydrogen bonding geometries are listed in Tables 2–4.

The orange-red isostructural binuclear complexes **1**, **2** and **3** contain crystallographic centers of inversion at the middle of the central N=N bond of the 4,4′-azpy molecule. In the crystal structures a solvent chloroform molecule is found in the asymmetric unit but in all three cases, the molecule is disordered with two overlapping molecules given population parameters *x* and 1 − *x* with *x* refined to values close to 0.5. In all the complexes each Mo(1) is bonded to two oxo atoms O(2) and O(3), phenolate oxygen O(1), thioenolate sulfur S(1), azomethine nitrogen N(1)

Table 1 Cyclic voltammetric results[a] (V *vs.* SCE) for the $[(Mo^{VI}O_2L)_2(4,4'\text{-azpy})]$ complexes at 298 K

Complexes	Mo(VI)–Mo(VI)/ Mo(IV)–Mo(IV) E_{pc} (V)	Mo(VI)–Mo(VI)/ Mo(IV)–Mo(IV) E_{pa} (V)
$[(MoO_2L^1)_2(4,4'\text{-azpy})]$ (**1**)	−0.92	+0.47
$[(MoO_2L^2)_2(4,4'\text{-azpy})]$ (**2**)	−0.98	+0.44
$[(MoO_2L^3)_2(4,4'\text{-azpy})]$ (**3**)	−1.01	+0.45

[a] Solvent: DMF (dry, degassed); supporting electrolyte: 0.1 M TBAP; solution strength: 10^{-3} M; working electrode: platinum; reference electrode: SCE; scan rate: 200 mV s^{-1}.

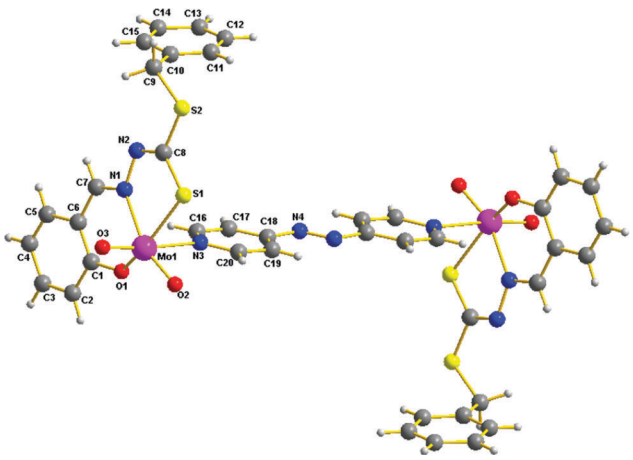

Fig. 1 View of the coordination environment around hexa-coordinated Mo(VI) with an atom labeling scheme in the centrosymmetric complex **1**, the disordered solvent molecule is omitted for clarity.

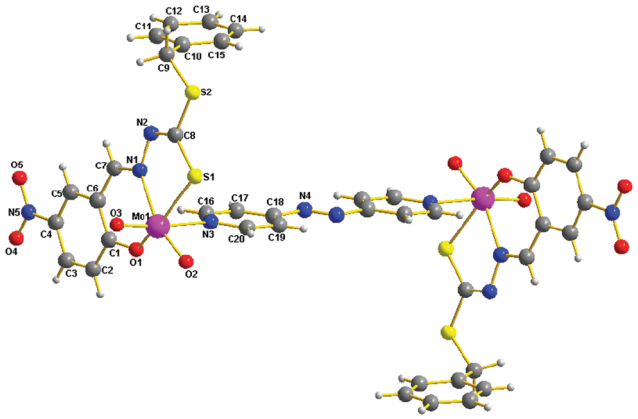

Fig. 2 View of the coordination environment around hexa-coordinated Mo(VI) with an atom labeling scheme in the centrosymmetric complex **2**, the disordered solvent molecule is omitted for clarity.

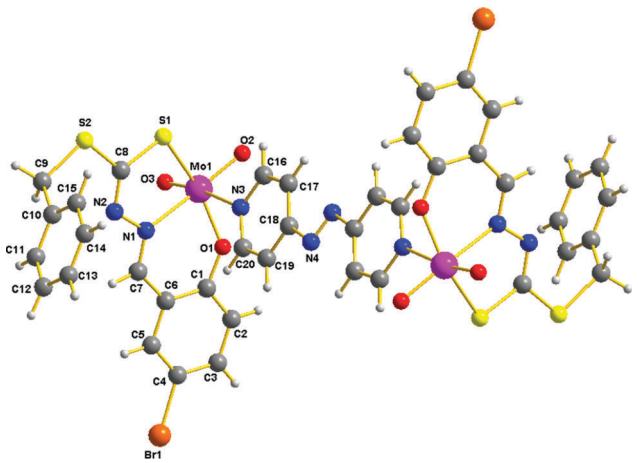

Fig. 3 View of the coordination environment around hexa-coordinated Mo(VI) with an atom labeling scheme in the centrosymmetric complex **3**, the disordered solvent molecule is omitted for clarity.

of the ligand and nitrogen atom N(3) of the bridging 4,4′-azpy molecule in a distorted octahedral coordination environment around the metal centre. The ligands are active in their enolate forms and behave in a dianionic tridentate manner. Three donor atoms O(1), N(1), and S(1) of the ligand and one terminal oxygen O(2) occupy the equatorial plane.[67] The dianionic tridentate ligands form one five-membered and another six-membered chelating ring around the $[MoO_2]^{2+}$ centre with bite angles of N(1)–Mo(1)–S(1), 75.8(2)°, 76.16(1)° and 75.98(1)° and N(1)–Mo(1)–N(3), 81.7(3)°, 81.87(1)° and 82.01(2)°, respectively. The oxo-oxygen O(3) occupies an axial position in the coordination sphere of Mo(1). The other axial position is occupied by the nitrogen atom N(3) of one half of the 4,4′-azpy unit. In complexes **1**, **2** and **3**, the Mo(VI) centre are displaced by 0.257, 0.268 and 0.328 Å, respectively, from the equatorial plane in the direction of the terminal oxygen O(3). The coordination mode of the Schiff base ligands allows the inclusion of the auxiliary ligand 4,4′-azpy which is an organic "distorted" rung[71] unit. The 4,4′-azpy ligand has four possible coordination sites, namely the two pyridine nitrogens and the two azo nitrogens. The molybdenum centre preferably coordinates to the two pyridine nitrogens since they are more readily accessible and also sterically favorable for the formation of binuclear complexes. The N-donor auxiliary ligand (4,4′-azpy) in **1–3** acts as a bis-monodentate ligand occupying one axial position and connecting two molybdenum(VI) atoms which are 13.816(2), 13.822(1) and 13.948(1) Å apart, respectively. No doubt because of the *trans* influence of O(3), the Mo(1)–N(3) bond lengths [2.435(8), 2.423(4) and 2.456(5) Å] are considerably longer than the other Mo(1)–N(1) bonds [2.259(8), 2.285(4) and 2.276(5) Å], values which indicate that the azpy nitrogen is comparatively weakly bonded to the $[MoO_2]^{2+}$ centre pointing to the possibility of ligand exchange reaction at this point. As the ligand is coordinated in the thiolate form, the C(8)–S(1) bond is expected to assume a single bond character but bond lengths are 1.709(10), 1.748(5) and 1.746(6) Å, respectively, distances which lie between the expected lengths of C–S and C=S bonds and may be attributed to electron delocalization in the coordinated ligands.[72,73] The adjacent C(8)–N(2) bond lengths are 1.289(11), 1.293(6) and 1.284(8) Å and are closer to the C=N distance than the normal C–N distance. The N(1)–N(2) bond distances 1.398(10), 1.409(5) and 1.410(7) Å, respectively, reveal their predominant single bond character.

Since the auxiliary ligand and the $[MoO_2L]$ layer are almost perpendicular to each other, interestingly considerable solvent-accessible voids between the layers are formed resulting in the formation of rhombus-shaped cavities. The cavities having dimensions 13.816 Å × 10.827 Å (**1**), 13.822 Å × 10.925 Å (**2**) and 13.948 Å × 11.180 Å (**3**) which are occupied by $CHCl_3$ molecules are further confirmed by TG and elemental analyses.

For a better understanding of the supramolecular framework formation, the various interactions present within the crystals are pictorially depicted in Fig. 4–6 for complexes **1**, **2** and **3**, respectively.

In complex **1**, the molybdenum oxo-oxygen (*trans* to 4,4′-azpy) and the coordinated sulphur behave as hydrogen bond acceptors. Adjacent binuclear complexes are linked *via* H(14)···O(3) and H(13)···S(1) hydrogen bonding interactions resulting in a chain type 2D supramolecular framework which propagates along the *a*-axis (Fig. S5, ESI†). Parallel chains further self-assemble *via* H(2)···O(2) hydrogen bonding interactions. The oxo-oxygen (*cis* to 4,4′-azpy) participates in hydrogen bonding interaction with the hydrogen of the salicylaldehyde ring finally leading to the construction of a 3D supramolecular pillared-layer framework (Fig. 7). The oxo-oxygens of the $[MoO_2]^{2+}$ moiety not only form hydrogen bonds to extend the chain structure but also behave as hydrogen bond acceptors to anchor the guest $CHCl_3$ molecules to the host framework *via* H(21)···O(3) and H(21)···O(2) interactions. Fig. S6 (ESI†) also portrays the staircase architecture of complex **1** along the *b*-axis.

Complex **2** is rich in hydrogen bonding interactions. The molybdenum oxo-oxygens are involved in hydrogen bonding interactions with hydrogen atoms in the phenyl ring of the *S*-benzyl moiety (Fig. S7, ESI†). Similar to complex **1**, here also the adjacent binuclear complexes are linked *via* H(13)···O(2) and H(12)···O(3) hydrogen bonding interactions resulting in an extended chain architecture along the *b*-axis (Fig. 8).

Table 2 Crystal data and details of refinement for complexes **1–3**

	Complex **1**	Complex **2**	Complex **3**
Chemical formula	$C_{42}H_{34}N_8S_4O_6Cl_6Mo_2$	$C_{42}H_{32}N_{10}S_4O_{10}Cl_6Mo_2$	$C_{42}H_{32}N_8\ S_4O_6Cl_6Br_2Mo_2$
Formula weight (M)	1279.59	1369.60	1437.38
Crystal system	Triclinic	Triclinic	Triclinic
Space group	$P\bar{1}$	$P\bar{1}$	$P\bar{1}$
a (Å)	10.827(18)	10.926(7)	11.166(5)
b (Å)	11.070(18)	10.964(7)	11.179(5)
c (Å)	12.580(2)	13.235(8)	13.139(6)
α (°)	65.780(17)	67.269(6)	67.863(10)
β (°)	73.533(17)	69.255(5)	65.724(10)
γ (°)	65.932(17)	67.937(6)	67.080(10)
V (Å^3)	1243(4)	1314(16)	1330.51(10)
Z	1	1	1
Crystal size	0.18 × 0.16 × 0.14	0.24 × 0.03 × 0.03	0.20 × 0.18 × 0.16
Temperature (K)	296(2)	150(2)	296(2)
D_C (g cm^{-3})	1.709	1.731	1.794
μ(Mo Kα) (mm^{-1})	1.050	1.006	2.484
F(000)	640	684	708
Goodness of fit on F^2	0.943	1.039	0.882
No of independent reflections	3437	7678	4959
No of reflections with $I > 2\sigma(I)$	2429	5698	3683
R_1, wR_2 [$I > 2\sigma(I)$]	R_1 = 0.0838	R_1 = 0.0590	R_1 = 0.0416
	wR_2 = 0.2067	wR_2 = 0.1243	wR_2 = 0.1037
Max, min residual electron density e Å^{-3}	1.204, −1.733	2.214, −2.235	1.072, −0.660

$R = \sum||F_0| - |F_c||/\sum|F_0|$; w$R(F^2) = [\sum w(|F_0|^2 - |F_c|^2)^2/\sum w|F_0|^4]^{1/2}$.

Table 3 Geometry of hydrogen-bonding interactions in the crystal structures of complexes **1–3**[a]

D–H	A	H···A (Å)	D···A (Å)	D–H···A (°)	Symmetry code
Complex **1**					
C(14)–H(14)	O(3)	2.92	3.78(2)	154.8	1 + x, y, z
C(13)–H(13)	S(1)	3.01	3.77(1)	140.7	1 + x, y, z
C(21A)–H(21A)	O(3)	2.72	3.47(2)	133.3	x, y, z
C(21A)–H(21A)	O(2)	2.38	3.16(2)	136.3	x, y, z
C(21B)–H(21B)	O(2)	2.62	3.40(2)	136.3	x, y, z
C(2)–H(2)	O(2)	2.69	3.90(2)	125.5	1 − x, −y, 1 − z
Complex **2**					
C(13)–H(13)	O(2)	2.88	3.52(2)	126.4	1 + x, y, z
C(12)–H(12)	O(3)	3.01	3.91(2)	162.3	1 + x, y, z
C(19)–H(19)	O(5)	2.47	3.39(2)	170.4	x, y, −1 + z
C(13)–H(13)	S(1)	3.10	3.82(1)	136.0	1 + x, y, z
C(21A)–H(21A)	O(3)	3.01	3.72(2)	130.3	1 − x, 1 − y, 1 − z
Complex **3**					
C(21A)–H(21A)	O(2)	2.22	3.33(2)	146.0	1 − x, −y, 2 − z
C(13)–H(13)	O(2)	2.82	3.49(2)	129.9	x, 1 + y, z
C(12)–H(12)	O(3)	3.12	4.01(1)	160.7	x, y, z
C(3)–H(3)	O(2)	2.83	3.41(2)	121.7	1 − x, −y, 2 − z

[a] C(21)–H(21) is a part of the chloroform molecule.

Parallel chains self assemble *via* H(19)···O(5) hydrogen bonding interactions. The oxygen atom of the nitro group helps to extend the chain to a 3D supramolecular framework with rhombus cavities (Fig. 8). The guest $CHCl_3$ molecules are entrapped in the rhombus cavities by H(21A)···O(3) hydrogen bonding interactions. In addition to the above described hydrogen bonding interactions that lead to framework formation, there are additional H(13)···S(1) hydrogen bonding interactions involving the coordinated sulphur and hydrogen atoms of the phenyl ring of the *S*-benzyl moiety which assist in the formation of a 3D robust framework.

Similarly in complex **3**, the oxo-oxygens actively participate in hydrogen bonding. The rhombus grid framework is basically formed by H(13)···O(2) and H(12)···O(3) hydrogen bonding interactions which help to extend the chain along the *b*-axis (Fig. S8, ESI†). The chains extend in three-dimensions by H(3)···O(2) hydrogen bonding interactions forming a fascinating supramolecular pillared layer structure (Fig. 9). The guest $CHCl_3$ molecules are held in the cavities (Fig. 6) by strong H(21)···O(2) hydrogen bonding interactions.

There are no π···π interactions in complexes **1–3** since the shortest centroid–centroid distances between adjacent aromatic rings are all >10 Å, much larger than those expected between the pyridyl rings for this type of interaction[20] [10.827 Å (**1**), 10.925 Å (**2**), and 11.180 Å (**3**)].

SEM investigations

The morphology and structure of the three binuclear dioxomolybdenum(VI) complexes **1–3** were examined using a scanning electron microscope. The samples were spread over a small piece of carbon tape and then coated with a 5 nm (approx.) thickness of Au using a BIO-RAD POLARAN sputter coater. The SEM images of the complexes are shown in Fig. 10. The images reveal that the compounds form crystalline structures in the form of microrods and microplates with dimensions of ∼2 μm. They have smooth surfaces and sharp edges and exhibit some degree of aggregation.

DFT and TD-DFT calculations of complexes 1, 2 and 3

The full geometry optimizations of **1**, **2** and **3** have been carried out using the DFT/B3LYP methodology. The calculated dimensions are

Table 4 X-ray and calculated (DFT/B3LYP method) bond distances (Å) and angles (deg) in **1–3**

	Complex **1**		Complex **2**		Complex **3**	
	Obs.	Calc.	Obs.	Calc.	Obs.	Calc.
Bond distances (Å)						
Mo(1)–O(1)	1.920(6)	1.980	1.961(3)	1.996	1.929(3)	1.983
Mo(1)–O(2)	1.692(6)	1.719	1.713(3)	1.717	1.703(3)	1.718
Mo(1)–O(3)	1.670(7)	1.707	1.700(3)	1.706	1.693(4)	1.707
Mo(1)–N(1)	2.259(9)	2.333	2.285(4)	2.340	2.285(4)	2.339
Mo(1)–N(3)	2.435(8)	2.544	2.423(4)	2.528	2.458(4)	2.538
Mo(1)–S(1)	2.416(4)	2.468	2.428(1)	2.457	2.435(2)	2.465
C(8)–S(1)	1.709(10)	1.760	1.748(5)	1.763	1.745(5)	1.761
C(8)–N(2)	1.289(11)	1.295	1.293(6)	1.296	1.282(6)	1.296
N(1)–N(2)	1.398(10)	1.383	1.409(5)	1.382	1.400(5)	1.380
Bond angles (deg)						
O(2)–Mo(1)–O(1)	106.0(3)	106.1	105.3(2)	106.2	104.9(2)	106.2
O(3)–Mo(1)–O(1)	99.5(3)	99.5	98.3(2)	98.6	99.6(2)	99.3
O(3)–Mo(1)–O(2)	105.5(3)	106.6	106.2(2)	106.5	105.8(2)	106.5
O(1)–Mo(1)–N(1)	81.7(3)	80.1	81.8(1)	80.0	82.1(1)	80.1
O(2)–Mo(1)–N(1)	160.2(3)	158.6	160.9(1)	159.6	160.6(2)	159.1
O(3)–Mo(1)–N(1)	90.9(3)	92.1	89.8(2)	91.4	90.4(2)	91.6
O(1)–Mo(1)–S(1)	150.6(2)	148	151.4(1)	148.1	151.5(1)	147.9
O(2)–Mo(1)–S(1)	90.3(3)	90.8	90.8(1)	91.3	90.9(1)	91.0
O(3)–Mo(1)–S(1)	99.5(3)	101.2	99.7(1)	101.6	98.4(2)	101.4
N(1)–Mo(1)–S(1)	75.8(2)	75.0	76.1(1)	75.1	75.9(1)	75.0
O(1)–Mo(1)–N(3)	76.8(3)	75.8	77.1(1)	75.9	77.5(1)	76.0
O(2)–Mo(1)–N(3)	82.4(3)	80.7	83.0(2)	81.1	82.5(2)	80.8
O(3)–Mo(1)–N(3)	172.0(3)	172.3	170.6(2)	171.8	171.6(2)	172.3
N(1)–Mo(1)–N(3)	81.7(3)	81.1	81.4(1)	81.6	81.4(1)	81.5
S(1)–Mo(1)–N(3)	81.4(2)	80.6	81.6(1)	80.9	81.4(1)	80.4
C(7)–N(1)–Mo(1)	124.6(7)	122.6	124.6(3)	122.8	124.(3)	122.8
N(2)–N(1)–Mo(1)	123.1(5)	122.9	122.5(3)	122.6	122.5(3)	122.8
C(16)–N(3)–Mo(1)	126.6(5)	123.7	124.1(3)	124.0	118.8(3)	117.5
C(20)–N(3)–Mo(1)	117.9(6)	117.9	118.8(3)	117.7	124.3(3)	124.2
C(1)–O(1)–Mo(1)	135.1(6)	131.4	135.9(3)	131.9	136.8(3)	131.6
C(8)–S(1)–Mo(1)	100.3(3)	100.7	100.1(2)	100.8	100.0(2)	100.7
O(1)–C(1)–C(6)	122.2(8)	122.0	121.9(4)	122.1	121.4(4)	122.1
C(1)–C(6)–C(7)	124.1(8)	123.0	123.7(4)	123.3	124.1(4)	123.2
N(1)–C(7)–C(6)	124.4(9)	126.3	125.9(4)	126.2	125.5(4)	126.2
C(7)–N(1)–N(2)	111.4(7)	113.6	112.2(4)	113.6	112.4(4)	113.6
C(8)–N(2)–N(1)	112.1(7)	114.6	113.0(4)	114.6	113.6(4)	114.6
N(2)–C(8)–S(1)	128.3(8)	126.5	127.5(4)	126.6	127.4(4)	126.5

given in Table 4 and are in good agreement with the experimental data. The maximum deviation in the bond length between experimental and calculated is 0.08–0.11 Å for Mo(1)–N(3).

The compositions along with the energies of some selected molecular orbitals of complexes are given in Tables S1–S3 (ESI†). Contour plots of some selected frontier molecular orbitals of the complexes are shown in Fig. 11–13. The higher energy occupied molecular orbitals (HOMO to HOMO−9) have significant contributions from ligand L, while HOMO−10 is concentrated on bridging the azpy moiety in the complexes. The lowest energy unoccupied molecular orbital (LUMO) has a π*(azpy) character. Other lowest energy unoccupied molecular orbitals (LUMO+1 to LUMO+8) have a mixed dπ(Mo) and π*(L) character along with a significant contribution from pπ(O) orbitals.

To obtain further insight into the electronic spectra of the complexes, vertical electronic excitations have been calculated by the TDDFT/CPCM method in dichloromethane solvent. The calculated excitation wavelengths and their assignments are summarized in Tables 5–7. In the complexes very weak transitions at 486–517 nm correspond to π(L) → π*(azpy) transitions. Again weak transitions at 440–470 nm have been observed for π(L) → π*(L)/dπ(Mo) transitions for **1** and **2**, while a mixed π(L) → π*(L)/dπ(Mo) and π(L) → π*(L)/π*(oxo) character in complex **3**. The moderately intense transitions at ∼400 nm have a π(L) → π*(azpy) character which has been experimentally observed for the complexes in dichloromethane. The high energy transitions at ∼300 nm again have π(L) → π*(azpy) in the complexes.

Antimicrobial activity

The Schiff base ligands and all the synthesized molybdenum(VI) complexes were tested against two gram-positive (*Bacillus cerus*, *Listeria monocytogenes*) and two gram-negative (*Escherichia coli*, *Staphylococcus aureus*) bacteria by the disc diffusion method. All the compounds exhibited different degrees of antimicrobial activity at a concentration of 10 μg per disc against the test pathogens. The qualitative and quantitative antimicrobial test results are presented in Tables 8 and 9 respectively. The antimicrobial activities were comparable with those of commonly used antibiotics (ampicillin and tetracycline) (reference disk) against the test pathogens. Among all the screened compounds,

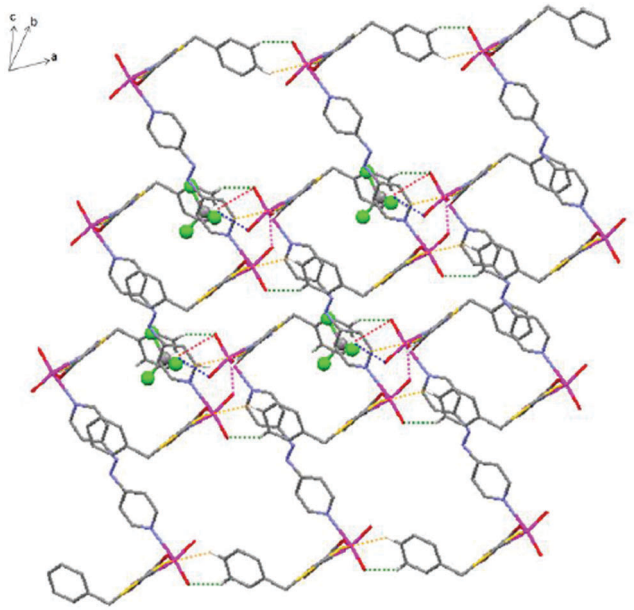

Fig. 4 Packing diagram of complex **1** showing the intermolecular hydrogen bonding interactions H(14)···O(3) (green dotted line), H(13)···S(1) (orange dotted line), H(21)···O(3) (red dotted line), H(21)···O(2) (blue dotted line) and H(2)···O(2) (magenta dotted line), non-bonding hydrogen atoms are omitted for clarity.

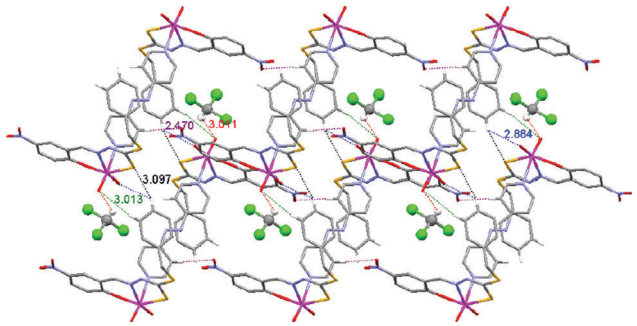

Fig. 5 Packing diagram of complex **2** along the *b*-axis showing the hydrogen bonding interactions H(13)···O(2) (blue dotted line), H(12)···O(3) (green dotted line), H(19)···O(5) (purple dotted line) H(13)···S(1) (black dotted line) and H(21A)···O(3) (red dotted line), non-bonding hydrogen atoms are omitted for clarity.

the Schiff base ligands ($\mathbf{H_2L^1}$–$\mathbf{H_2L^3}$) showed moderate to good antimicrobial activity against all these test microorganisms. Complex **1** showed moderate to good activity against *Escherichia coli* and *Listeria monocytogenes* and exhibited weak activity against other test organisms. Complex **2** showed good activity against the tested pathogens and complex **3** also showed moderate activities against the pathogens. From Table 8 it is observed that ligands $\mathbf{H_2L^1}$–$\mathbf{H_2L^3}$ have better antimicrobial activity than their corresponding complexes. The Schiff base ligands were also found to have comparable activity to the two established drugs against the bacterial strains studied under the test conditions, showing that they have a good activity as bactericides.

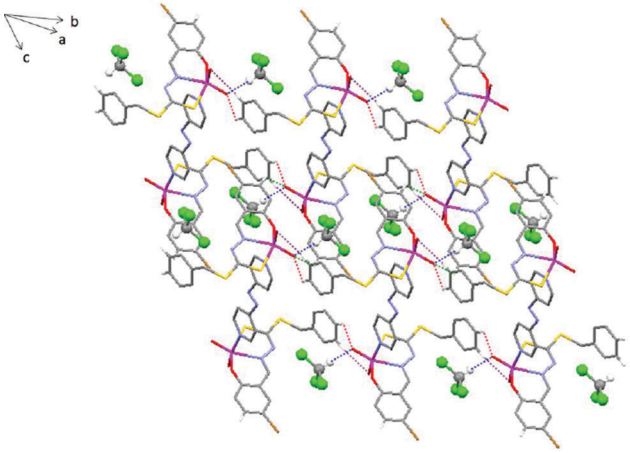

Fig. 6 Packing diagram of complex **3** showing the hydrogen bonding interactions H(21)···O(2) (blue dotted line), H(13)···O(2) (red dotted line), H(12)···O(3) (purple dotted line) and H(3)···O(2) (green dotted line), non-bonding hydrogen atoms are omitted for clarity.

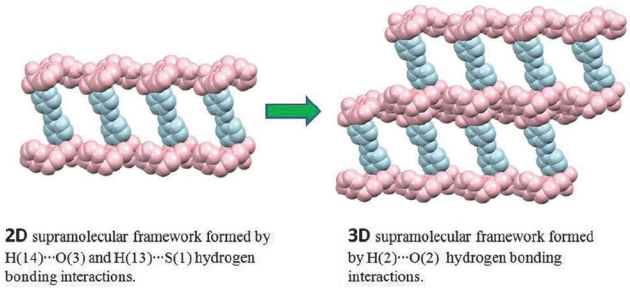

Fig. 7 Spacefilling representation illustrating the formation of a supramolecular pillared-layer structure in complex **1**, the azpy pillars are shown in blue and the MoO_2L^1 layer is shown in pink, hydrogen atoms and solvent molecules are omitted for clarity.

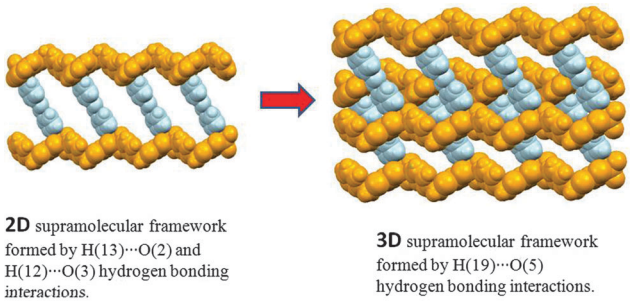

Fig. 8 Spacefilling representation illustrating the formation of a supramolecular pillared-layer structure in complex **2**, the azpy pillars are shown in blue and the MoO_2L^2 layer is shown in orange, hydrogen atoms and solvent molecules are omitted for clarity.

The MIC of the ligands and their corresponding molybdenum complexes against the test microorganisms was further determined using sterilized discs saturated with different concentrations (0.25–10 μg per disc) of test compounds. The MIC value of the compounds for antimicrobial activity ranges

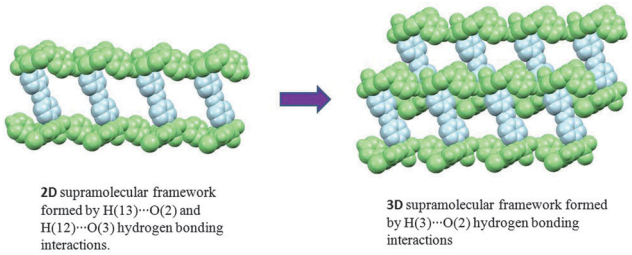

Fig. 9 Spacefilling representation illustrating the formation of a supramolecular pillared-layer structure in complex **3**, the azpy pillars are shown in blue and the MoO_2L^3 layer is shown in green, hydrogen atoms and solvent molecules are omitted for clarity.

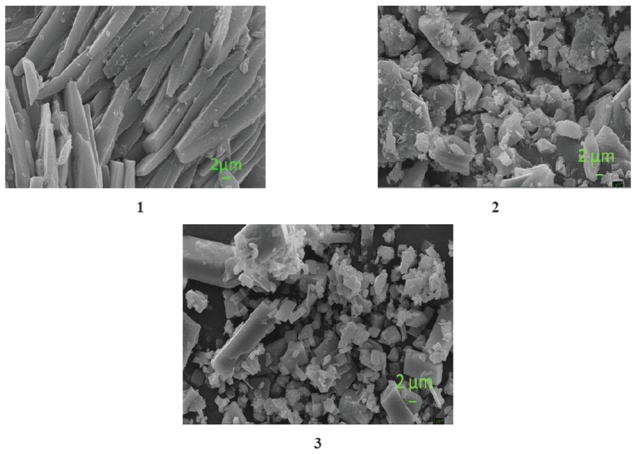

Fig. 10 SEM images of complexes **1**, **2** and **3**.

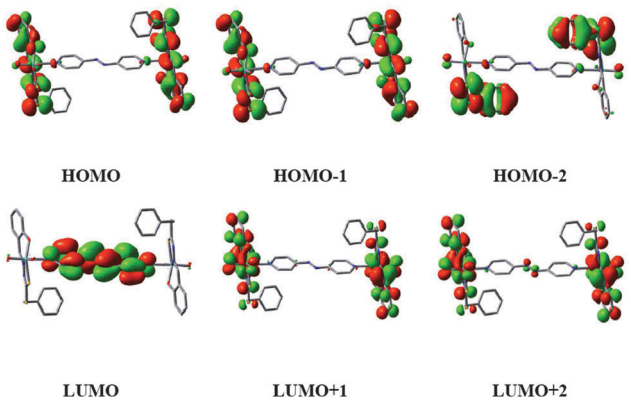

Fig. 11 Contour plots of selected molecular orbitals of complex **1**.

between 0.5 and 10 μg per disc (Table 9). The results reveal that the Schiff base ligands[74–76] and the synthesized complexes **1–3** may be proposed as potential new candidates in antimicrobial treatment. Thus, from the MIC and average inhibition zone results, it is revealed that $\mathbf{H_2L^1}$ and $\mathbf{H_2L^2}$ posses the highest activity among all the compounds against the test microorganisms. A graphical representation of the inhibition zones of the compounds is given in Fig. 14.

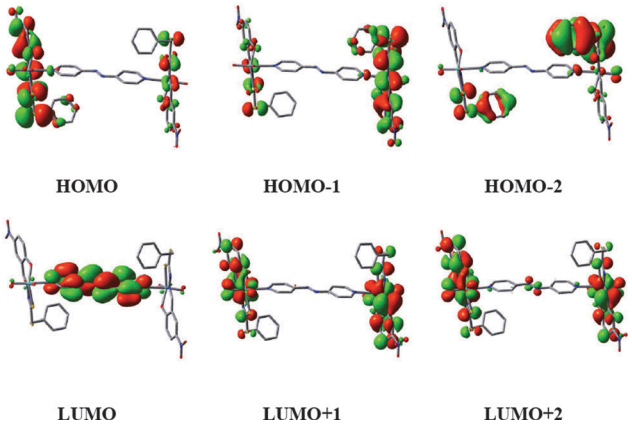

Fig. 12 Contour plots of selected molecular orbitals of complex **2**.

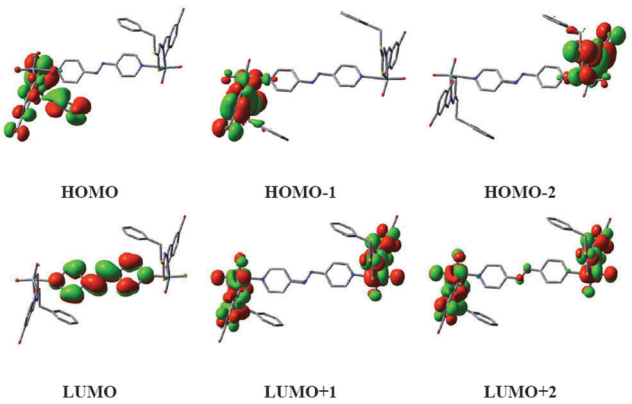

Fig. 13 Contour plots of selected molecular orbitals of complex **3**.

Antioxidant activity

The model of the scavenging of a stable DPPH (2,2-diphenyl-1-picrylhydrazyl) radical is commonly employed for the assay of antioxidant activity of compounds across a short time scale. The use of the stable DPPH radical (due to extensive delocalization of the unpaired electron) has the advantage of being less affected by side reactions such as enzyme inhibition and metal chelation.[77] DPPH accepts an electron or hydrogen to become a stable diamagnetic radical. Due to its unpaired electron, DPPH gives a strong absorption band at 517 nm giving a deep violet colour.[78] As the electron becomes paired up in the presence of the Schiff base ligands ($\mathbf{H_2L^1}$–$\mathbf{H_2L^2}$) and complexes **1–3**, the absorption diminishes giving a yellow colour and this resulting decolourization is stoichiometric with respect to the number of electrons taken up. With the increase in concentration of the test compounds a marked decrease in absorption was observed indicating strong antioxidant properties of the test compounds.

The total antioxidant capacity (TAC) of the compounds in terms of the ascorbic acid equivalent (AAE) is given in Table 10 and DPPH radical scavenging activity is given in Table 11. Ligand $\mathbf{H_2L^2}$ gave the best results for total antioxidant capacity assay as 1 mg of sample was equivalent to 0.09 mg of ascorbic

Table 5 Calculated vertical electronic excitations in complex **1**

$E_{excitation}$ (eV)	$\lambda_{excitation}$ (nm)	Osc. strength (f)	Key transitions	Character
2.4002	516.6	0.0140	(92%) HOMO → LUMO	$\pi(L^1) \rightarrow \pi^*$(azpy)
2.6628	465.6	0.0471	(49%) HOMO−1 → LUMO+1	$\pi(L^1) \rightarrow \pi^*(L^1)/d\pi$(Mo)
			(41%) HOMO → LUMO+2	
2.9688	417.6	0.0719	(74%) HOMO−4 → LUMO	$\pi(L^1) \rightarrow \pi^*$(azpy)
3.2172	385.4	0.0423	(86%) HOMO−8 → LUMO	$\pi(L^1) \rightarrow \pi^*$(azpy)
3.5175	352.5	0.4260	(33%) HOMO → LUMO+6	$\pi(L^1) \rightarrow \pi^*(L^1)/d\pi$(Mo)
			(27%) HOMO−1 → LUMO+5	
3.7006	335.0	0.0513	(67%) HOMO−11 → LUMO	$\pi(L^1) \rightarrow \pi^*$(azpy)
4.0353	307.3	0.2163	(65%) HOMO−12 → LUMO	$\pi(L^1) \rightarrow \pi^*$(azpy)

Table 6 Calculated vertical electronic excitations in complex **2**

$E_{excitation}$ (eV)	$\lambda_{excitation}$ (nm)	Osc. strength (f)	Key transitions	Character
2.5520	485.8	0.0202	(78%) HOMO−1 → LUMO	$\pi(L^2) \rightarrow \pi^*$(azpy)
2.7652	448.4	0.0185	(34%) HOMO−1 → LUMO+1	$\pi(L^2) \rightarrow \pi^*(L^2)/d\pi$(Mo)
			(32%) HOMO−1 → LUMO+2	
2.7671	448.1	0.0266	(34%) HOMO → LUMO+1	$\pi(L^2) \rightarrow \pi^*(L^2)/d\pi$(Mo)
			(32%) HOMO → LUMO+2	
2.8680	432.3	0.0240	(81%) HOMO−2 → LUMO	$\pi(L^2) \rightarrow \pi^*$(azpy)
3.1720	390.9	0.1293	(73%) HOMO−6 → LUMO	$\pi(L^2) \rightarrow \pi^*$(azpy)
3.3352	371.75	0.0457	(48%) HOMO−9 → LUMO	$\pi(L^2) \rightarrow \pi^*$(azpy)
3.7309	332.3	0.0845	(39%) HOMO → LUMO+6	$\pi(L^2) \rightarrow \pi^*(L^2)/d\pi$(Mo)
			(25%) HOMO−1 → LUMO+5	
4.1159	301.2	0.0792	(65%) HOMO−11 → LUMO	$\pi(L^2) \rightarrow \pi^*$(azpy)

Table 7 Calculated vertical electronic excitations in complex **3**

$E_{excitation}$ (eV)	$\lambda_{excitation}$ (nm)	Osc. strength (f)	Key transitions	Character
2.4088	514.72	0.0102	(85%) HOMO → LUMO	$\pi(L^3) \rightarrow \pi^*$(azpy)
2.6436	468.99	0.0234	(45%) HOMO−1 → LUMO+1	$\pi(L^3) \rightarrow \pi^*(L^3)/d\pi$(Mo)
			(40%) HOMO → LUMO+2	$\pi(L^3) \rightarrow \pi^*(L^3)/\pi^*$(oxo)
2.6499	467.88	0.0251	(43%) HOMO−1 → LUMO+1	$\pi(L^3) \rightarrow \pi^*(L^3)/d\pi$(Mo)
			(41%) HOMO−1 → LUMO+3	$\pi(L^3) \rightarrow d\pi$(Mo)/ π^*(oxo)
2.9596	418.92	0.0491	(90%) HOMO−4 → LUMO	$\pi(L^3) \rightarrow \pi^*$(azpy)
3.2152	385.62	0.0752	(69%) HOMO−8 → LUMO	$\pi(L^3) \rightarrow \pi^*$(azpy)
3.2469	381.86	0.0208	(34%) HOMO−5 → LUMO+3	$\pi(L^3) \rightarrow d\pi$(Mo)/$\pi^*$(oxo)
3.3839	366.40	0.0344	(32%) HOMO−3 → LUMO+4	$\pi(L^3) \rightarrow d\pi$(Mo)/$\pi^*$(oxo)
3.6550	339.2	0.0692	(35%) HOMO−1 → LUMO+5	$\pi(L^3) \rightarrow \pi^*(L^3)/d\pi$(Mo)
			(29%) HOMO → LUMO+6	
4.1065	301.9	0.0812	(72%) HOMO−12 → LUMO	$\pi(L^3) \rightarrow \pi^*$(azpy)

Table 8 Antimicrobial activity of the ligands and complexes **1–3**

	Test pathogens (average inhibition zone in mm)			
Compounds (10 μg per disc)	*Escherichia coli*	*Bacillus subtilis*	*Listeria monocytogenes*	*Staphylococcus aureus*
$\mathbf{H_2L^1}$	19.5	12	18	9
1	14	7	12	8
$\mathbf{H_2L^2}$	17	14	20	8
2	16	13	16	—
$\mathbf{H_2L^3}$	15	13	11	10
3	10	11	10	8.5
Ampicillin	14	—	30	—
Tetracycline	—	—	18	24

[—] = no inhibition; [NT] = not tested.

Table 9 Minimum inhibitory concentration (MIC) (μg per disc) of the ligands and complexes **1–3**

	Test pathogens			
Compounds	*Escherichia coli*	*Bacillus subtilis*	*Listeria monocytogenes*	*Staphylococcus aureus*
$\mathbf{H_2L^1}$	0.5	0.5	0.5	1
1	0.5	5	1	1
$\mathbf{H_2L^2}$	0.5	0.5	0.5	1
2	0.5	1	0.5	10
$\mathbf{H_2L^3}$	0.5	0.5	0.5	1
3	1	0.5	0.5	1

acid. Moreover, $\mathbf{H_2L^2}$ had 76.56% DPPH radical scavenging capacity which is the highest among the six compounds analyzed at a low concentration of 50 μg ml^{-1}.

Conclusions

We have successfully synthesized three new isostructural binuclear dioxomolybdenum(VI) complexes by using Schiff base ligands together with 4,4′-azopyridine as the spacer. All three

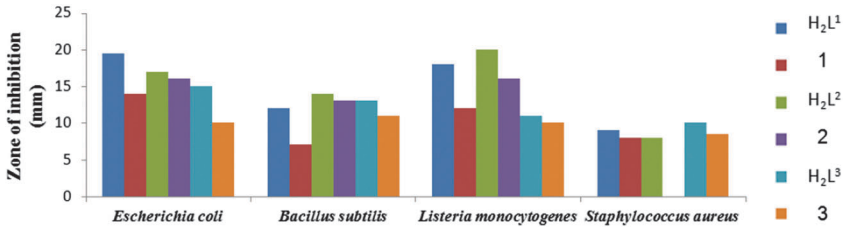

Fig. 14 Zone of inhibition (mm) of the compounds(10 μg per disc) for the pathogens.

Table 10 TAC values of the ligands and complexes **1–3**

	H_2L^1	1	H_2L^2	2	H_2L^3	3
TAC (AAE) (mg mg^{-1})	0.08	0.06	0.09	0.06	0.09	0.06

Table 11 DPPH radical scavenging activity of the ligands and complexes **1–3**

	H_2L^1	1	H_2L^2	2	H_2L^3	3
Inhibition (%) at 50 μg ml^{-1} conc.	64.41	17.21	76.56	29.05	57.01	24.38

complexes have been characterized by single crystal X-ray crystallography and thermal analysis. The X-ray crystallographic study reveals that the hydrogen bonding interactions play a pivotal role in the construction of supramolecular frameworks. The pillaring role of the 4,4′-azopyridine spacer is particularly important as it not only fixes the neighboring 2D layers with an appropriate distance and prevent the clogging of channels but also adjust the size of cavities in the frameworks. Thus, the 4,4′-azopyridine spacer has been shown to be a good candidate for the construction of supramolecular assemblies. The rhombus-shaped cavities in the complexes make them potential candidates for gas adsorption, ion-sensing, *etc.* Thermal studies reveal the robustness of frameworks. Relevant DFT calculations on the ligands and complexes were also carried out and the data were used to identify the composition of the relevant HOMOs and LUMOs and also to assign experimentally observed transitions. SEM images show highly crystalline structures in the form of microrods and microplates. The electrochemical study shows an irreversible redox behaviour of all the binuclear dioxomolybdenum(VI) complexes. These complexes are of special relevance due to the intriguing supramolecular architectures. Schiff base ligands $\mathbf{H_2L^1}$ and $\mathbf{H_2L^2}$ show good antimicrobial activity against the four bacterial strains. Ligand $\mathbf{H_2L^3}$ and complexes **1–3** also exhibit significant antimicrobial activity. All the Schiff base ligands were found to be effective antioxidants of the DPPH radical. Among all the compounds, ligand $\mathbf{H_2L^2}$ gave best antioxidant activity.

Acknowledgements

D. Biswal acknowledges UGC, New Delhi, for the senior research fellowship. The authors thank the University of Reading and the EPSRC (U.K) for funds for the Oxford Diffraction diffractometer, Dr Ganesh C. Sahoo (CSIR-CGCRI) for the thermal analysis and Dr Pramit Chowdhury (IIT Delhi) for the SEM study. S. Biswas acknowledges UGC, New Delhi, and T. K. Mondal acknowledge DST, New Delhi.

References

1 V. Vrdoljak, D. Milić, M. Cindrić, D. M. Čalogović, J. Pisk, M. Marković and P. Novak, *Z. Anorg. Allg. Chem.*, 2009, **635**, 1242–1248.
2 I. Sheikhshoaie, A. Rezaeifard, N. Monadi and S. Kaafi, *Polyhedron*, 2009, **28**, 733–738.
3 A. Rezaeifard, I. Sheikhshoaie, N. Monadi and M. Alipour, *Polyhedron*, 2010, **29**, 2703–2709.
4 S. Pasayat, S. P. Dash, P. K. Majhi, Y. P. Patil, M. Nethaji, H. R. Dash, S. Das and R. Dinda, *Polyhedron*, 2012, **38**, 198–204.
5 R. D. Chakravarthy, K. Suresh, V. Ramkumar and D. K. Chand, *Inorg. Chim. Acta*, 2011, **376**, 57–63.
6 A. Capapé, M.-D. Zhou, S.-L. Zang and F. E. Kühn, *J. Organomet. Chem.*, 2008, **693**, 3240–3244.
7 C. D. Brondino, M. J. Romão, I. Moura and J. J. Moura, *Curr. Opin. Chem. Biol.*, 2006, **10**, 109–114.
8 N. Kanoongo, R. V. Singh, J. P. Tandun and R. B. Goyal, *J. Inorg. Biochem.*, 1990, **38**, 57–67.
9 D. Biswal, N. R. Pramanik, S. Chakrabarti, N. Chakraborty, K. Acharya, S. S. Mandal, S. Ghosh, M. G. B. Drew, T. K. Mondal and S. Biswas, *New J. Chem.*, 2015, **39**, 2778–2794.
10 B. Booth, T. Donnelly and A. Letter, *Biochem. Pharmacol.*, 1971, **20**, 3109–3118.
11 C. Carini, G. Pelizzi, P. Torasconi, C. Pelizzi, K. C. Molloy and P. C. Watertield, *J. Chem. Soc., Dalton Trans.*, 1989, 289–293.
12 R. K. Grasselli, *Catal. Today*, 1999, **49**, 141.
13 R. J. Cross, P. D. Newman, R. D. Peacock and D. Stirling, *J. Mol. Catal.*, 1999, **144**, 273–284.
14 K. J. Ivin and J. C. Mol, *Olefin Metathesis Polymerization*, Academic Press, London, 1997.
15 N. Gharah, S. Chakraborty, A. K. Mukherjee and R. Bhattacharyya, *Chem. Commun.*, 2004, 2630–2632.
16 N. R. Pramanik, M. Chakraborty, D. Biswal, S. S. Mandal, S. Ghosh, S. Chakrabarti, W. S. Sheldrick, M. G. B. Drew, T. K. Mondal and D. Sarkar, *Polyhedron*, 2015, **85**, 196–207.
17 C. S. Marvel and N. Tarkoy, *J. Am. Chem. Soc.*, 1957, **79**, 6000.
18 R. Dinda, S. Ghosh, L. R. Falvello, M. Tomas and T. C. W. Mak, *Polyhedron*, 2006, **25**, 2375–2382.

19 B. K. Koo, H. Kang and W. T. Lim, *Bull. Korean Chem. Soc.*, 2008, **29**, 1819–1822.
20 P. Kar, R. Biswas, M. G. B. Drew, A. Frontera and A. Ghosh, *Inorg. Chem.*, 2012, **51**, 1837–1851.
21 T. Koshiyama, M. Shirai, T. Hikage, H. Tabe, K. Tanaka, S. Kitagawa and T. Ueno, *Angew. Chem., Int. Ed.*, 2011, **50**, 4849–4852.
22 D. Maspoch, D. Ruiz-Molina and J. Veciana, *Chem. Soc. Rev.*, 2007, **36**, 770–818.
23 B. Bhattacharya, R. Halder, R. Dey, T. K. Maji and D. Ghoshal, *Dalton Trans.*, 2014, **43**, 2272–2282.
24 (*a*) J. Kim, H. Furukawa, N. Ko, Y. B. Go, N. Aratani, S. B. Choi, E. Choi, A. O. Yazaydin, R. Q. Snurr, M. O'Keeffe and O. M. Yaghi, *Science*, 2010, **329**, 424–428; (*b*) C. Y. Lee, O. K. Farha, B. J. Hong, A. A. Sarjeant, S. T. Nguyen and J. T. Hupp, *J. Am. Chem. Soc.*, 2011, **133**, 15858–15861; (*c*) Y. E. Cheon and M. P. Suh, *Chem. Commun.*, 2009, 2296–2298; (*d*) P. Kanoo, R. Matsuda, M. Higuchi, S. Kitagawa and T. K. Maji, *Chem. Mater.*, 2009, **21**, 5860–5866.
25 (*a*) M. Eddaoudi, D. B. Moler, H. L. Li, B. L. Chen, T. M. Reineke, M. O'Keeffe and O. M. Yaghi, *Acc. Chem. Res.*, 2001, **34**, 319–330; (*b*) M. E. Kosal, J. H. Chou, S. R. Wilson and K. S. Suslick, *Nat. Mater.*, 2002, **1**, 118–121; (*c*) L. Pan, D. H. Olson, L. R. Ciemnolonski, R. Heady and J. Li, *Angew. Chem., Int. Ed.*, 2006, **45**, 616–619; (*d*) Z. Zhang, Y. Zhao, Q. Gong, Z. Li and J. Li, *Chem. Commun.*, 2013, **49**, 653–661; (*e*) S. S. Nagarkar, A. K. Chaudhuri and S. K. Ghosh, *Inorg. Chem.*, 2012, **51**, 572–576; (*f*) S. Keksin, T. M. van Heest and D. S. Sholl, *ChemSusChem*, 2010, **3**, 879–891.
26 (*a*) P. Horcajada, C. Serre, G. Maurin, N. A. Ramsahye, F. Balas, M. Vallet-Regi, M. Sebban, F. Taulelle and G. Ferey, *J. Am. Chem. Soc.*, 2008, **130**, 6774–6780; (*b*) J. Y. An, S. J. Geib and N. L. Rosi, *J. Am. Chem. Soc.*, 2009, **131**, 8376–8377; (*c*) N. J. Hinks, A. C. McKinlay, B. Xiao, P. S. Wheatley and R. E. Morris, *Microporous Mesoporous Mater.*, 2010, **129**, 330–334.
27 (*a*) D. Saha, R. Sen, T. Maity and S. Koner, *Dalton Trans.*, 2012, **41**, 7399–7408; (*b*) M. Fujita, Y. J. Kwon, S. Washizu and K. Ogura, *J. Am. Chem. Soc.*, 1994, **116**, 1151–1152; (*c*) C. D. Wu, A. Hu, L. Zhang and W. Lin, *J. Am. Chem. Soc.*, 2005, **127**, 8940–8941.
28 F. A. Cotton, G. Wilkinson, C. A. Murillo and M. Bochmann, *Advanced Inorganic Chemistry*, Wiley, Chichester, 6th edn, 1999.
29 J. T. Lin, S.-S. Sun, J. J. Wu, L. Lee, K. J. Lin and Y. F. Huang, *Inorg. Chem.*, 1995, **34**, 2323–2333.
30 N. K. Ngan, K. M. Lo and C. S. R. Wong, *Polyhedron*, 2012, **33**, 235–251.
31 (*a*) Q. Chu, Z. Su, J. Fan, T. A. Okamura, G. C. Lv, G. X. Liu, W. Y. Sun and N. Ueyama, *Cryst. Growth Des.*, 2011, **11**, 3885–3894; (*b*) O. K. Farha, C. D. Malliakas, M. G. Kanatzidis and J. T. Hupp, *J. Am. Chem. Soc.*, 2010, **132**, 950–952.
32 (*a*) C. M. Nagaraja, R. Haldar, T. K. Maji and C. N. R. Rao, *Cryst. Growth Des.*, 2012, **12**, 975–981; (*b*) S. Q. Zhang, F. L. Jiang, M. Y. Wu, J. Ma, Y. Bu and M. C. Hong, *Cryst. Growth Des.*, 2012, **12**, 1452–1463; (*c*) M. Deniz, I. Hernandez-Rodriguez, J. Pasan, O. Fabelo, L. Canadillas-Delgado, C. Yuste, M. Julve, F. Lloret and C. Ruiz-Perez, *Cryst. Growth Des.*, 2012, **12**, 4505–4518.
33 E. V. Brown and G. R. Granneman, *J. Am. Chem. Soc.*, 1975, **97**, 621–627.
34 N. R. Pramanik, S. Ghosh, T. K. Raychaudhuri, S. Ray, R. J. Butcher and S. S. Mandal, *Polyhedron*, 2004, **23**, 1595–1603.
35 *SAINT*, Bruker AXS Inc., Madison, Wisconsin, USA, 2007.
36 *CrysAlis*, Oxford Diffraction Ltd, Abingdon, U.K., 2006.
37 G. M. Sheldrick, Shelxs97 and Shelxl97, Programs for Crystallographic solution and refinement, *Acta Crystallogr., Sect. A: Found. Crystallogr.*, 2008, **64**, 112–122.
38 G. M. Sheldrick, *SADABSs, An empirical absorption correction program*, Bruker AXS Inc., Madison, Wisconsin, USA, 2001.
39 *ABSPACK*, Oxford Diffraction Ltd, Oxford, U.K., 2005.
40 C. F. Macrae, P. R. Edington, P. McCabe, E. Pidcock, G. P. Shields, R. Taylor, M. Towler and J. van de Streck, *J. Appl. Crystallogr.*, 2006, **39**, 453–457.
41 K. Brandenburg, *DIAMOND*, Crystal Impact GbR, Bonn, Germany, 1999.
42 A. D. Becke, *J. Chem. Phys.*, 1993, **98**, 5648–5652.
43 C. Lee, W. Yang and R. G. Parr, *Phys. Rev. B: Condens. Matter Mater. Phys.*, 1988, **37**, 785–789.
44 P. J. Hay and W. R. Wadt, *J. Chem. Phys.*, 1985, **82**, 270–283.
45 W. R. Wadt and P. J. Hay, *J. Chem. Phys.*, 1985, **82**, 284–298.
46 P. J. Hay and W. R. Wadt, *J. Chem. Phys.*, 1985, **82**, 299–310.
47 R. Bauernschmitt and R. Ahlrichs, *Chem. Phys. Lett.*, 1996, **256**, 454–464.
48 R. E. Stratmann, G. E. Scuseria and M. J. Frisch, *J. Chem. Phys.*, 1998, **109**, 8218–8224.
49 M. E. Casida, C. Jamorski, K. C. Casida and D. R. Salahub, *J. Chem. Phys.*, 1998, **108**, 4439–4449.
50 V. Barone and M. Cossi, *J. Phys. Chem. A*, 1998, **102**, 1995–2001.
51 M. Cossi and V. Barone, *J. Chem. Phys.*, 2001, **115**, 4708–4717.
52 M. Cossi, N. Rega, G. Scalmani and V. Barone, *J. Comput. Chem.*, 2003, **24**, 669–681.
53 M. J. Frisch, G. W. Trucks, H. B. Schlegel, G. E. Scuseria, M. A. Robb, J. R. Cheeseman, G. Scalmani, V. Barone, B. Mennucci, G. A. Petersson, H. Nakatsuji, M. Caricato, X. Li, H. P. Hratchian, A. F. Izmaylov, J. Bloino, G. Zheng, J. L. Sonnenberg, M. Hada, M. Ehara, K. Toyota, R. Fukuda, J. Hasegawa, M. Ishida, T. Nakajima, Y. Honda, O. Kitao, H. Nakai, T. Vreven, J. A. Montgomery, Jr., J. E. Peralta, F. Ogliaro, M. Bearpark, J. J. Heyd, E. Brothers, K. N. Kudin, V. N. Staroverov, R. Kobayashi, J. Normand, K. Raghavachari, A. Rendell, J. C. Burant, S. S. Iyengar, J. Tomasi, M. Cossi, N. Rega, J. M. Millam, M. Klene, J. E. Knox, J. B. Cross, V. Bakken, C. Adamo, J. Jaramillo, R. Gomperts, R. E. Stratmann, O. Yazyev, A. J. Austin, R. Cammi, C. Pomelli, J. W. Ochterski, R. L. Martin, K. Morokuma, V. G. Zakrzewski, G. A. Voth, P. Salvador,

J. J. Dannenberg, S. Dapprich, A. D. Daniels, Ö. Farkas, J. B. Foresman, J. V. Ortiz, J. Cioslowski and D. J. Fox, *Gaussian 09, Revision D.01*, Gaussian, Inc., Wallingford, CT, 2009.
54 N. M. O'Boyle, A. L. Tenderholt and K. M. Langner, *J. Comput. Chem.*, 2008, **29**, 839–845.
55 A. W. Bauer, W. M. M. Kirby, J. C. Sherris and M. Turck, *Am. J. Clin. Pathol.*, 1966, **45**(4), 493–496.
56 P. Prieto, M. Pineda and M. Aguilar, *Anal. Biochem.*, 1999, **269**, 337–341.
57 K. Shimada, K. Fujikawa, K. Yahara and T. Nakamura, *J. Agric. Food Chem.*, 1992, **40**(6), 945–948.
58 E. I. Stiefel, *Prog. Inorg. Chem.*, 1977, **22**, 1.
59 Y.-L. Zhai, X.-X. Xu and X. Wang, *Polyhedron*, 1992, **11**, 415–418.
60 A. Syamal and K. S. Kale, *Inorg. Chem.*, 1965, **4**, 867–873.
61 M. Goodgame and P. J. Hayward, *J. Chem. Soc. A*, 1966, 632–634.
62 Y.-L. Zhai, X.-X. Xu and X. Wang, *Polyhedron*, 1992, **11**, 415–418.
63 M. Chaudhury, *J. Chem. Soc., Dalton Trans.*, 1984, 115–120.
64 R. H. Holm, P. Kennepohl and E. I. Solomon, *Chem. Rev.*, 1996, 2239–2314.
65 S. Bhattacharyya, S. B. Kumar, S. K. Dutta, E. R. T. Tiekink and M. Chaudhury, *Inorg. Chem.*, 1996, **35**, 1967–1973.
66 M. Chaudhury, *Inorg. Chem.*, 1985, **24**, 3011–3017.
67 R. Hahn, U. Kusthardt and W. Scherer, *Inorg. Chim. Acta*, 1993, **210**, 177–182.
68 R. Mattes and V. Mikloweit, *Inorg. Chim. Acta*, 1986, **122**, L19–L20.
69 A. P. Koley, S. Purohit, S. Ghosh, L. S. Prasad and P. T. Manoharan, *J. Chem. Soc., Dalton Trans.*, 1988, 2607–2613.
70 S. Purohit, A. P. Koley, L. S. Prasad, P. T. Manoharan and S. Ghosh, *Inorg. Chem.*, 1989, **28**, 3735–3742.
71 K. Otsubo, A. Kobayashi, K. Sugimoto, A. Fujiwara and H. Kitagawa, *Inorg. Chem.*, 2014, **53**, 1229–1240.
72 M. W. Bishop, J. Chatt, J. R. Dilworth, M. B. Hursthouse, S. Amarasiri, A. Jayaweera and A. Quick, *J. Chem. Soc., Dalton Trans.*, 1979, 914–920.
73 M. W. Bishop, J. Chatt, J. R. Dilworth, M. B. Hursthouse and M. Motevalli, *J. Chem. Soc., Dalton Trans.*, 1979, 1603–1606.
74 M. Ali, A. Mirza, R. Butcher, M. Tarafder, B. Tan and A. Ali, *J. Inorg. Biochem.*, 2002, **92**, 141.
75 T. B. S. A. Ravoof, K. A. Crouse, M. Ibrahim, M. Tahir, A. R. Cowley and M. Akbar Ali, *Polyhedron*, 2004, **23**, 2491–2498.
76 M. Tofazzal, H. Tarafdar, M. Akbar Ali, D. J. Wee, K. Azahari, S. Silong and K. A. Crouse, *Transition Met. Chem.*, 2000, **25**, 456–460.
77 R. Amarowicz, R. B. Pegg, P. Rahimi-Moghaddam, B. Barl and J. A. Weil, *Food Chem.*, 2004, **84**, 551–562.
78 D. N. Nicolaides, D. R. Gautam, K. E. Litinas, D. J. Hadjipavlou-Litina and K. C. Fylaktakidou, *Eur. J. Med. Chem.*, 2004, **39**, 323–332.

